

Harmonic generation predominantly from a single spin channel in a half metal

G. P. Zhang*

Department of Physics, Indiana State University, Terre Haute, Indiana 47809, USA

Y. H. Bai

Office of Information Technology, Indiana State

University, Terre Haute, Indiana 47809, USA

(Dated: March 10, 2021)

Abstract

Harmonic generation in atoms and molecules has reshaped our understanding of ultrafast phenomena beyond the traditional nonlinear optics and has launched attosecond physics. Harmonics from solids represents a new frontier, where both majority and minority spin channels contribute to harmonics. This is true even in a ferromagnet whose electronic states are equally available to optical excitation. Here, we demonstrate that harmonics can be generated mostly from a single spin channel in half metallic chromium dioxide. An energy gap in the minority channel greatly reduces the harmonic generation, so harmonics predominantly emit from the majority channel, with a small contribution from the minority channel. However, this is only possible when the incident photon energy is well below the energy gap in the minority channel, so all the transitions in the minority channel are virtual. The onset of the photon energy is determined by the transition energy between the dipole-allowed transition between the O- $2p$ and Cr- $3d$ states. Harmonics mainly from a single spin channel can be detected, regardless of laser field strength, as far as the photon energy is below the minority band energy gap. This prediction should be tested experimentally.

PACS numbers: 42.65.Ky, 78.66.Tr

Keywords:

I. INTRODUCTION

Rapid developments of high harmonic generation (HHG) in atoms and molecules [1, 2] have opened new frontiers in material research and ultrafast science. Starting from 1990s, interest has shifted from atoms, molecules to nanostructure and actual solids [3–10]. Solids are much more complex, and they demand more from HHG. For instance, can HHG directly probe band structures in a solid [11–13]? Developing harmonics into a tool to explore properties in topological materials such as Bi_2Se_3 [14, 15], MnBi_2Te_4 [16], MoS_2 [17] and spin-orbit coupled systems [18] is particularly important, given that vast majority of devices are solids. Up to now, most of materials investigated so far are nonmagnetic and most of them are insulators and semiconductors [7, 9, 19]. In ferromagnets, both majority and minority spin channels contribute to harmonic signals [20], so it is difficult to disentangle their respective contributions cleanly [21]. In antiferromagnets, one encounters the same difficulty where two sublattices with opposite spin orientations both contribute to harmonic signals [22]. So far, pure spin polarized harmonics in solids have not materialized, but are in huge demand in materials where spin dynamics is important. In laser-induced ultrafast demagnetization [23, 24], one needs to know how differently two spin channels evolve with time. THz emission was reported in $\text{Cr}(30 \text{ \AA})/\text{Ni}(42 \text{ \AA})/\text{Cr}(70 \text{ \AA})$ films [25], and more recently in $\text{Co}/\text{ZnO}/\text{Pt}$ and $\text{Co}/\text{Cu}/\text{Pt}$ multilayers [26] and $\text{MgO}/\text{Fe}/\text{MgO}$ thin films [27]. THz emission only allows one to access magnetization on a picosecond time scale. Being able to detect the spin signal from harmonics beyond THz emission potentially provides a new way to investigate spin wave dynamics [28, 29] on a few hundred femtoseconds.

In this paper, we demonstrate harmonic generation mostly from a single spin channel in half metallic CrO_2 [30, 31]. CrO_2 has no energy gap in the majority spin channel, but has a gap in the minority one. The minority state is away from the Fermi level and the spin-orbit coupling is weak, leading to nearly 100% spin polarization [32]. These interesting properties manifest themselves in harmonic generation. The energy gap in the minority band limits the efficiency of harmonic generation, but the effect on each order of harmonics is different. The fundamental harmonic, the first harmonic, is weakly affected, and has no strong dependence on the incident laser photon energy. A much stronger effect is found in higher orders of harmonics. With the laser parameters used, we find that upon excitation of a 0.4-eV pulse, the fifth harmonic from the majority channel is 60 times stronger than

that from the minority signal, making it a nearly pure single-spin channel harmonic. This difference disappears when a higher photon energy is used. Such a dramatic effect is closely related to the dipole-allowed transitions between the oxygen $2p$ states and chromium $3d$ state, where the strongest transition is slightly above 2 eV. It is generally believed that harmonic generation does not have the spin selectivity. Our finding here demonstrates that optical harmonics can be a powerful tool to access spin information in half-metals, where harmonics are largely emitted from a single spin channel.

The rest of the paper is arranged as follows. In Sec. II, we present our theoretical formalism. The results and discussions are in Sec. III. We conclude this paper in Sec. IV.

II. THEORETICAL FORMALISM

We employ the first-principles density functional theory and couple it to the time-dependent Liouville equation. This formalism represents an important alternative to the time-dependent density functional theory and rigorously respects the Pauli exclusion principles [33]. Here in brief, we solve the the spin-polarized Kohn-Sham equation [34–37],

$$\left[-\frac{\hbar^2 \nabla^2}{2m_e} + V_{ne} + V_{ee} + V_{xc} \right] \psi_{i\mathbf{k}}^\sigma(\mathbf{r}) = E_{i\mathbf{k}}^\sigma \psi_{i\mathbf{k}}^\sigma(\mathbf{r}), \quad (1)$$

where σ is the spin index, m_e is the electron mass, the terms on the left-hand side represent the kinetic energy, nuclear-electron attraction, electron-electron Coulomb repulsion and exchange correlation (generalized gradient approximation [38]), respectively. $\psi_{i\mathbf{k}}^\sigma(\mathbf{r})$ is the Bloch wavefunction of band i for spin σ at crystal momentum \mathbf{k} , and $E_{i\mathbf{k}}^\sigma$ is the band energy. Our two spin channels are not mixed because of weak spin-orbit coupling [32]. This allows us to cleanly investigate the contributions from these two spin channels. We use the full-potential augmented plane wave method as implemented in the Wien2k code [34], where within the Muffin-tin sphere atomic basis functions are used and in the interstitial region a plane wave is used. These two basis functions are matched both in value and slope at the Muffin-tin boundary.

To investigate high harmonic generation, we solve the Liouville equation in real time. Different from prior studies [39], we have to solve the equation for each spin channel σ ,

$$\frac{\partial \rho_{\mathbf{k}}^\sigma}{\partial t} = \frac{1}{i\hbar} [H_0^\sigma + H_I^\sigma, \rho_{\mathbf{k}}^\sigma] - \frac{\rho_{\mathbf{k}}^\sigma - \rho_{\mathbf{k}}^\sigma(0)}{T_{1(2)}}, \quad (2)$$

so the computational cost doubles. Here $\rho_{\mathbf{k}}^{\sigma}$ is the time-dependent density matrix with spin σ at the \mathbf{k} point and $\rho_{\mathbf{k}}^{\sigma}(0)$ is its initial value. The second term on the right side describes the decay of the density matrix to its initial value [40]. For a diagonal density matrix element $\rho_{\mathbf{k};ii}^{\sigma}$, the second term becomes $-\rho_{\mathbf{k};ii}^{\sigma} + \rho_{\mathbf{k};ii}^{\sigma}(0)/T_1$, where i is the band index and T_1 is called the longitudinal relaxation time. For an off-diagonal density matrix element $\rho_{\mathbf{k};i\neq j}^{\sigma}$, the second term is $-\rho_{\mathbf{k};i\neq j}^{\sigma}/T_2$, where i and j are the band indices and T_2 is called the transverse relaxation time. Note that the initial off-diagonal matrix elements are zero. T_1 and T_2 are different from those in NMR where T_1 is used for the z component of magnetization M_z and T_2 is used for the x and y components [41]. H_0 is the field-free system Hamiltonian. H_I^{σ} represents the interaction between the laser field and system, $H_I^{\sigma} = -\sum_{\mathbf{k};i,j} \rho_{\mathbf{k};i,j}^{\sigma} \mathbf{P}_{\mathbf{k};j,i}^{\sigma} \cdot \mathbf{A}(t)$. $\mathbf{P}_{\mathbf{k};i,j}^{\sigma}$ is the momentum matrix element between bands i and j at the \mathbf{k} point, and is calculated within the Wien2k code, but these matrix elements must be converted properly before use (see the details in Ref. [42]). $\mathbf{A}(t)$ is the vector potential, $\mathbf{A}(t) = A_0 \sin^2(t/\tau)(\cos(\omega t)\hat{x} \pm \sin(\omega t)\hat{y})$, where A_0 is the amplitude of the vector potential in units of Vfs/Å [20], \hat{x} and \hat{y} are the unit vectors along the x and y axes, respectively, t is the time, ω is the carrier frequency, $+$ and $-$ refer to the left (σ^-) and right (σ^+) circularly polarized light within the xy plane, respectively. τ is the laser pulse duration. We choose the duration τ to be 64 cycles of laser period [5]. This is sufficient to resolve harmonics at different orders. If the laser polarization is within the yz plane, those unit vectors must be changed properly.

III. RESULTS AND DISCUSSIONS

CrO₂ crystallizes in the rutile structure, with the space group P4₂/mnm. The Cr atoms form a body-centered tetragonal lattice. If we orient the structure in such a way that the Cr atom is at the center of the oxygen distorted octahedron, then two apex oxygen atoms O_1 and O_2 are placed along the vertical direction. Four equatorial oxygen atoms O_3, \dots , and O_6 , whose Wyckoff positions are $(u, u, 0)$, $(u, u, 1)$, $(1 - u, 1 - u, 0)$, and $(1 - u, 1 - u, 1)$, are placed in the horizontal plane. The distance between the body center Cr atom and O_1 and O_2 is shorter, $d_a = 1.8962\text{\AA}$, and that between the body center Cr atom and O_3, \dots , and O_6 is longer, $d_e = 1.9087\text{\AA}$, both of which are computed from $d_a = \sqrt{2}ua$ and $d_e = \sqrt{2(\frac{1}{2} - u)^2a^2 + (c/2)^2}$ [43]. There are two distances between neighboring O

atoms, c and $\sqrt{2}(2u-1)a$, and normally they differ, so one does not have an ideal octahedron.

Our \mathbf{k} mesh is $29 \times 29 \times 45$, with 2760 points in the irreducible Brillouin zone. The product of planewave cutoff K_{\max} and Muffin-tin radius R_{MT} , $R_{\text{MT}}K_{\max}$, determines the accuracy of our calculation. Our $R_{\text{MT}}K_{\max}$ is 9, which is more than enough for our purpose. $R_{\text{MT}}(\text{Cr})$ is 1.89 a.u. and $R_{\text{MT}}(\text{O})$ is 1.67 a.u. We optimize the internal coordinates of atoms, and we compare our results with the experimental ones in Table I. We see that the agreement with the experiment is excellent. Our theoretical spin moment for formula unit is $2.0 \mu_B$, which agrees with the experimental result of $2.0 \mu_B$ nearly perfectly and prior theoretical calculations [30, 43].

Figure 1(a) displays the partial density of states (PDOS) for the majority (positive value) and minority (negative value) spins. The solid line and dotted line denote the Cr-3d and O-2p majority states, respectively. The vertical dashed line represents the Fermi energy which is set at 0. One sees that both Cr-3d and O-2p states cross the Fermi level, which is why CrO₂ is a metal. Each cell has 28 valence majority electrons and 24 minority electrons. The Fermi energy nearly cuts at the local minimum of Cr-3d states, stabilizing CrO₂ [43]. The minority PDOS is quite different (see the solid and dashed lines on the negative axis). At the Fermi level, there is no DOS, with a band gap of 1.43 eV [30]. These features are fully consistent with prior studies [30, 43, 44]. What is important for harmonic generation is that the valence band is dominated by the O-2p state, while the conduction band is dominated by the Cr-3d state. This constitutes an ideal case for dipole-allowed transitions.

We find there is no major difference between left and right circularly polarized light for our system, so in the following we use σ^+ , with the photon energy 0.4 eV and field amplitude $A_0 = 0.03$ Vfs/Å. Our interested observable is the expectation value of the momentum operator, $\langle \mathbf{P}^\sigma(t) \rangle = \langle \sum_{\mathbf{k};i,j} \rho_{\mathbf{k};i,j}^\sigma \mathbf{P}_{\mathbf{k};j,i}^\sigma \rangle$, where the summation is over the Brillouin zone and band states. In our calculation, we include all the states from Cr-3s states (energy at -4.89 Ry for spin up and -4.73 Ry for spin down), Cr-3p state (energy at -2.79 Ry for spin up and -2.64 Ry for spin down), O-2s (-0.95 Ry), all the way up to 4.95 Ry, with 10 Ry energy window width covering all the possible channels for excitation. To compute harmonic spectra, we Fourier transform $\langle \mathbf{P}^\sigma(t) \rangle$ into the frequency domain [5, 17, 20],

$$\mathbf{P}(\Omega) = \int_{-\infty}^{\infty} \mathbf{P}(t) e^{i\Omega t} \mathcal{W}(t) dt, \quad (3)$$

where $\mathcal{W}(t)$ is the window function [20].

Figure 1(b) shows harmonic signals from the majority (top) and minority (bottom) spin channels, respectively. We see that all the harmonics appear at odd orders because our system has an inversion symmetry. The majority spin channel has a stronger harmonic signal than the minority spin channel, and it has a broader peak. This difference is expected from the PDOS. Recall that the minority band has an energy gap, so with the photon energy of 0.4 eV, the excitation is virtual. The majority band has no such gap, so electrons in the valence band can successively excite into conduction bands and then emit harmonics.

We notice a crucial difference when we compare the 3rd harmonic signal with the 5th harmonic signal from the majority and minority spin channels. The difference in the 5th harmonic between the majority and minority spin channels is much larger. A very weak 5th harmonic in the minority channel is interesting because it potentially provides an opportunity to generate harmonics from a single spin channel. We note that in a nonmagnetic material [14], there is no difference in harmonics between spin up and spin down channels. In ferromagnets, this difference is also small because each channel is able to generate harmonics with a small difference in strength [16, 17, 20]. A challenge in ferromagnetic metals is that the electron deexcitation is extremely fast [20], so it is difficult to detect those harmonics. CrO₂ is very unique. It is known that laser-induced ultrafast demagnetization lasts very long [45], partly because its spin-orbit coupling is very weak. This prolonged process is advantageous to detect harmonic signals.

Next we investigate how laser parameters affect harmonic generation in CrO₂. We increase the photon energy to 0.8 eV, while keeping the rest of laser parameters unchanged. Figure 2(b) shows that the 5th harmonic in the minority channel at 0.8 eV is slightly smaller than that in the majority channel, very different from that at 0.4 eV (see Fig. 2(a)). Energetically, when the photon energy $\hbar\omega$ is 0.4 eV, $5\hbar\omega = 2$ eV is slightly above the gap energy of 1.43 eV. Because a transition from the O-2*p* to Cr-3*d* does not occur immediately at this band gap energy, one is still in the virtual excitation regime. This situation is important because not all half metals have this property. For instance, in another half-metal, Mn₂RuGa does not have this unique feature, so its harmonic generation from the majority channel is similar to that in the minority channel. With $\hbar\omega = 0.8$ eV, $5\hbar\omega = 4$ eV is well into the real excitation regime, so the band gap suppression is no longer at work. This is further verified when we increase the incident photon energy to 1.6 eV. Figure 2(c) shows that harmonic strength in the minority and majority channels is almost exactly the same, so harmonics are

generated from both spin channels. Figure 2(d) compares the harmonic signal ratio of the majority harmonic signal to the minority harmonic signal as a function of incident photon energy. We see that in general higher order harmonics have a much stronger variation. The ratio is larger when the incident photon energy is small. At 0.4 eV, the fifth harmonic has a ratio of 67 with $A_0 = 0.03\text{Vfs}/\text{\AA}$. This photon energy window predicted here is critical to future experiments.

To show that our prediction is not specific to a particular laser field strength, we choose several vector potential amplitudes. We increase the amplitude A_0 from 0.01 to 0.05 Vfs/ \AA and include both the third and fifth harmonics. Figure 3(a) displays the third harmonic signal as a function of A_0 for spin up (filled circles) and spin down (filled boxes) channels. The photon energy is 0.4 eV and the duration is also 64 cycles of the laser period as above. We see that both signals increase superlinearly. We fit the signal to a power function and find that the signal scales with A_0 as $A_0^{2.37}$. According to the traditional nonlinear optics [40], the polarization \mathcal{P} is proportional to the response function $R(t)$ multiplied by the external field $E(t)$ [46], and for the third harmonic $\mathcal{P}^{(3)} \propto R^{(3)}(t)E(t)^3$. If $R^{(3)}(t)$ is significantly modulated by band states, the scaling exponent differs from 3. This shows that real excitations among band states contribute to the harmonic signal, which is exactly what one expects from the density of states in the spin majority channel (Fig. 1(a)). The spin minority channel is different. We see that the signal scales as $A_0^{2.99}$ (filled boxes in Fig. 3(a)), with the exponent close to 3. This again shows that the excitation is virtual, as expected.

Different excitations seen above also leave a crucial hallmark on the power spectrum as well. Figure 3(b) shows the third harmonic signal as a function of A_0 , from 0.01 to 0.05 Vfs/ \AA , denoted respectively by the circles, boxes, diamonds, up triangles and left triangles. We see that the peaks for the spin up channel are not entirely symmetric with respect to the 3rd order. This is an indication that harmonics are generated through real states (Fig. 1). In the spin down channel, the harmonic peak is highly symmetric (see Fig. 3(c)). In other words, the harmonic asymmetry is a hallmark for transitions that involve real band states, which is crucial for electronic structure detection in solids.

We can further demonstrate this in the fifth harmonic. Figure 3(d) shows the 5th harmonic signal as a function of A_0 for the majority spin (circles) and minority spin (boxes) channels. As we increase A_0 , the signal scales as $A_0^{4.32}$, indicative of real transitions among band states. To reveal further details in harmonics, we also plot the harmonic spectrum.

Figure 3(e) shows that the harmonic peak is not symmetric with respect to 5. All the harmonic signals are multiplied by 100 for an easy view. In the spin down channel, we note that the nominal 5th peak does not appear at 5 (Fig. 3(f)), where harmonic signals are multiplied by 1000 for an easy view. This is because the main excitation occurs above 2 eV, which is fully consistent with our observation in the photon energy dependence in Fig. 2. In comparison with the majority signal, the minority signal is extremely weak even at 0.05 Vfs/Å. Quantitatively, we find the ratio between the majority and minority 5th order signals is 46, or about 2%.

To establish our results on a solid ground, we carry out several additional tests. We first check our harmonic signal convergence with the Brillouin zone sampling by increasing the number of k points from $18 \times 18 \times 28$, $19 \times 19 \times 30$, to $29 \times 29 \times 45$, and we find the results are well converged. For all the results in this paper, we use a \mathbf{k} mesh of $29 \times 29 \times 45$, with 2760 points in the irreducible Brillouin zone, or 10830 in the full Brillouin zone. Secondly, we examine the influence of relaxation times T_1 and T_2 on the harmonic signal. T_2 is normally shorter than T_1 , but their precise values are unknown, so to this end, we take $T_1 = 200$ fs and $T_2 = 100$ fs. Extremely smaller T_1 and T_2 were used before in ZnO [47]. Figures 4(a)-(d) show the results for the same laser parameters used in Fig. 1(a), but with $T_1 = 400$ fs and $T_2 = 200$ fs. Their influence on our harmonic signal is very weak since our laser pulse duration is on the order of 200 fs. When we increase T_1 and T_2 from 200 and 100 fs to 400 and 200 fs, the fifth order harmonic changes from 0.36×10^{-2} to 0.50×10^{-2} for the majority channel. The change is even smaller for the minority band, and it only changes from 0.55×10^{-4} to 0.52×10^{-4} for the minority channel in the same unit. This huge difference between the spin majority and minority channels remains, regardless of the x (Figs. 4(a) and 4(c)) or y (Figs. 4(b) and (d) or Figs. 4(e) and 4(f)) or z component (Figs. 4(f) and 4(h)). Since CrO₂ is tetragonal, we wonder whether the laser polarization in the yz plane (σ_{yz}), instead of the xy plane (σ_{xy}), makes a difference. Figures 4(e)-(h) show our results with the same relaxation times as Figs. 4(a)-(d). We find that for the majority band, the y component maximum of the 5th harmonic signal is similar, but the line shape is slightly different. Under σ_{yz} excitation, the peak appears more symmetric (see Fig. 4(e)) and has no structure in it, while under σ_{xy} excitation, the peak has more structures. This difference is due to the different band states involved during harmonic generation. This potentially provides another interesting direction for experimental investigation as a function of laser polarization angle,

in a similar way as done in MgO [19]. For the minority band, the difference is much smaller (see Figs. 4(g) and 4(f)). Importantly, the ratio of the majority 5th harmonic to that of the minority remains the same. This concludes that the fifth order harmonic emission is mainly from the majority channel. This paves the way to future experimental detection of harmonics from a single spin channel. We believe that the results found here are interesting and should motivate future experimental and theoretical investigations.

IV. CONCLUSION

We have investigated harmonic generation from half-metallic CrO₂. This nearly 100% spin polarized material shows peculiar features that are not found in other materials. The majority spin channel has no energy gap just like a metal, but in the minority channel has 1.4-eV energy gap. Upon laser excitation, this leads to a significant difference in harmonic generation in these two channels. This difference depends on the harmonic order and photon energy $\hbar\omega$ used. The higher the order is, the larger the effect is. At $\hbar\omega = 0.4$ eV and the fifth harmonic, we find that the ratio of the majority channel signal to the minority signal exceeds 60. This makes the 5th harmonic as if it is emitted nearly purely from a single spin channel. Microscopically, in the minority channel, transitions are mainly from the O-2*p* states to Cr-3*d* states, so the onset of single spin channel harmonics starts at 2 eV. This explains why the fifth order shows such a strong effect. In general, it is known that harmonics are less sensitive to material properties. Here, we show that when a material has a peculiar difference in spin channels, harmonics can be very powerful. Our prediction, if confirmed experimentally, potentially represents a new direction for high harmonic generation for solids [7–10, 48].

Acknowledgments

This work was solely supported by the U.S. Department of Energy under Contract No. DE-FG02-06ER46304. Part of the work was done on Indiana State University’s high performance Quantum and Obsidian clusters. The research used resources of the National Energy Research Scientific Computing Center, which is supported by the Office of Science of the U.S. Department of Energy under Contract No. DE-AC02-05CH11231.

- [1] A. McPherson, G. Gibson, H. Jara, U. Johann, T. S. Luk, I. A. McIntyre, K. Boyer, and C. K. Rhodes, Studies of multiphoton production of vacuum-ultraviolet radiation in the rare gases, *J. Opt. Soc. Am. B* **4**, 595 (1987),
- [2] M. Ferray, A. L’Huillier, X. F. Li, L. A. Lompre, G. Mainfray, and C. Manus, Multiple-harmonic conversion of 1064 nm radiation in rare gases, *J. Phys. B: At. Mol. Opt. Phys.* **21**, L31 (1988).
- [3] Gy. Farkas, Cs. Tóth, S. D. Moustazis, N. A. Papadogiannis, and C. Fotakis, Observation of multiple-harmonic radiation induced from a gold surface by picosecond neodymium-doped yttrium aluminum garnet laser pulses, *Phys. Rev. A* **46**, R3605 (1992).
- [4] D. von der Linde, T. Engers, G. Jenke, P. Agostini, G. Grillon, E. Nibbering, A. Mysyrowicz, and A. Antonetti, Generation of high-order harmonics from solid surfaces by intense femtosecond laser pulses, *Phys. Rev. A* **52**, R25 (1995).
- [5] G. P. Zhang, Optical high harmonic generations in C_{60} , *Phys. Rev. Lett.* **95**, 047401 (2005).
- [6] R. Ganeev, L. Bom, J. Abdul-Hadi, M. Wong, J. Brichta, V. Bhardwaj, and T. Ozaki, Higher-order harmonic generation from fullerene by means of the plasma harmonic method, *Phys. Rev. Lett.* **102**, 013903 (2009).
- [7] S. Ghimire, E. Sistrunk, P. Agostini, L. F. DiMauro, and D. A. Reis, Observation of high-order harmonic generation in a bulk crystal, *Nat. Phys.* **7**, 138 (2011).
- [8] T. T. Luu, M. Garg, S. Yu. Kruchinin, A. Moulet, M. Th. Hassan, and E. Goulielmakis, Extreme ultraviolet high-harmonic spectroscopy of solids, *Nature* **521**, 498 (2015).
- [9] M. Garg, M. Zhan, T. T. Luu, H. Lakhotia, T. Klostermann, A. Guggenmos, and E. Goulielmakis, Multi-petahertz electronic metrology, *Nature* **538**, 359 (2016).
- [10] G. Ndabashimiye, S. Ghimire, M. Wu, D. A. Browne, K. J. Schafer, M. B. Gaarde, and D. A. Reis, Solid-state harmonics beyond the atomic limit, *Nature* **534**, 520 (2016).
- [11] G. Vampa, T. J. Hammond, N. Thire, B. E. Schmidt, F. Legare, C. R. McDonald, T. Brabec, D. D. Klug, and P. B. Corkum, All-optical reconstruction of crystal band structure, *Phys. Rev. Lett.* **115**, 193603 (2015).
- [12] G. Vampa, C. R. McDonald, G. Orlando, P. B. Corkum and T. Brabec, Semiclassical analysis

- of high harmonic generation in bulk crystals, *Phys. Rev. B* **91**, 064302 (2015).
- [13] G. P. Zhang and Y. H. Bai, High-order harmonic generation in solid C_{60} , *Phys. Rev. B* **101**, 081412(R) (2020).
- [14] L. Jia, Z. Zhang, D. Z. Yang, M. S. Si, G. P. Zhang, and Y. S. Liu, High harmonic generation in magnetically doped topological insulators, *Phys. Rev. B* **100**, 125144 (2019).
- [15] D. Baykusheva, A. Chacon, D. Kim, D. E. Kim, D. A. Reis, and S. Ghimire, Strong-field physics in three-dimensional topological insulators, *Phys. Rev. A* **103**, 023101 (2021).
- [16] L. Jia, Z. Zhang, D. Z. Yang, M. S. Si, and G. P. Zhang, Probing magnetic configuration-mediated topological phases via high harmonic generation in $MnBi_2Te_4$, *Phys. Rev. B* **102**, 174314 (2020).
- [17] L. Jia, Z. Zhang, D. Z. Yang, Y. Liu, M. S. Si, G. P. Zhang, and Y. S. Liu, Optical high-order harmonic generation as a structural characterization tool, *Phys. Rev. B* **101**, 144304 (2020).
- [18] M. Lysne, Y. Murakami, M. Schüler, and P. Werner, High-harmonic generation in spin-orbit coupled systems, *Phys. Rev. B* **102**, 081121(R) (2020).
- [19] Y. S. You, D. A. Reis and S. Ghimire, Anisotropic high-harmonic generation in bulk crystals, *Nature Phys.* **13**, 345 (2017).
- [20] G. P. Zhang, M. S. Si, M. Murakami, Y. H. Bai, and T. F. George, Generating high-order optical and spin harmonics from ferromagnetic monolayers, *Nat. Commun.* **9**, 3031 (2018).
- [21] S. Takayoshi, Y. Murakami, and P. Werner, High-harmonic generation in quantum spin systems, *Phys. Rev. B* **99**, 184303, (2019).
- [22] N. Tancogne-Dejean, M. A. Sentef, and A. Rubio, Ultrafast modification of Hubbard U in a strongly correlated material: *ab initio* high-harmonic generation in NiO, *Phys. Rev. Lett.* **121**, 097402 (2018).
- [23] E. Beaurepaire, J. C. Merle, A. Daunois, and J.-Y. Bigot, Ultrafast spin dynamics in ferromagnetic nickel, *Phys. Rev. Lett.* **76**, 4250 (1996).
- [24] G. P. Zhang, W. Hübner, E. Beaurepaire, and J.-Y. Bigot, Laser-induced ultrafast demagnetization: Femtomagnetism, A new frontier? *Topics Appl. Phys.* **83**, 245 (2002).
- [25] E. Beaurepaire, G. M. Turner, S. M. Harrel, M. C. Beard, J.-Y. Bigot, and C. A. Schmuttenmaer, Coherent terahertz emission from ferromagnetic films excited by femtosecond laser pulses, *Appl. Phys. Lett.* **84**, 3465 (2004).
- [26] G. Li, R. V. Mikhaylovskiy, K. A. Grishunin, J. D. Costa, Th. Rasing, and A. V. Kimel,

- Laser induced THz emission from femtosecond photocurrents in Co/ZnO/Pt and Co/Cu/Pt multilayers, *J. Phys. D: Appl. Phys.*, **51**, 134001 (2018).
- [27] W. Zhang, P. Maldonado, Z. Jin, T. S. Seifert, J. Arabski, G. Schmerber, E. Beaurepaire, M. Bonn, T. Kampfrath, P. M. Oppeneer, and D. Turchinovich, Ultrafast terahertz magnetometry, *Nat. Commun.* **11**, 4247 (2020).
- [28] Q. Zhang, A. V. Nurmikko, A. Anguelouch, G. Xiao and A. Gupta, Coherent magnetization rotation and phase control by ultrashort optical pulses in CrO₂ thin films, *Phys. Rev. Lett.* **89**, 177402 (2002).
- [29] G. M. Müller, J. Walowski, M. Djordjevic, G.-X. Miao, A. Gupta, A. V. Ramos, K. Gehrke, V. Moshnyaga, K. Samwer, J. Schmalhorst, A. Thomas, A. Hütten, G. Reiss, J. S. Moodera, and M. Münzenberg, Spin polarization in half-metals probed by femtosecond spin excitation, *Nat. Mater.* **8**, 56 (2009).
- [30] K.-H. Schwarz, CrO₂ predicted as a half-metallic ferromagnet, *J. Phys. F: Met. Phys.* **16**, L211 (1986).
- [31] J. M. D. Coey, *Magnetism and Magnetic Materials*, Cambridge University Press (2010).
- [32] R. J. Soulen Jr., J. M. Byers, M. S. Osofsky, B. Nadgorny, T. Ambrose, S. F. Cheng, P. R. Broussard, C. T. Tanaka, J. Nowak, J. S. Moodera, A. Barry, and J. M. D. Coey, Measuring the spin polarization of a metal with a superconducting point contact, *Science* **282**, 85 (1998).
- [33] G. P. Zhang, Y. H. Bai, and T. F. George, Ultrafast reduction of exchange splitting in ferromagnetic nickel, *J. Phys.: Condens. Matt.* **28**, 236004 (2016).
- [34] P. Blaha, K. Schwarz, G. K. H. Madsen, D. Kvasnicka, and J. Luitz, WIEN2k, An Augmented Plane Wave + Local Orbitals Program for Calculating Crystal Properties (Karlheinz Schwarz, Techn. Universität Wien, Austria, 2001).
- [35] P. Blaha, K. Schwarz, F. Tran, R. Laskowski, G. K. H. Madsen and L. D. Marks, WIEN2k: An APW+lo program for calculating the properties of solids, *J. Chem. Phys.* **152**, 074101 (2020).
- [36] G. P. Zhang, W. Hübner, G. Lefkidis, Y. Bai, and T. F. George, Paradigm of the time-resolved magneto-optical Kerr effect for femtosecond magnetism, *Nat. Phys.* **5**, 499 (2009).
- [37] G. P. Zhang, Y. H. Bai, and T. F. George, Energy- and crystal momentum-resolved study of laser-induced femtosecond magnetism, *Phys. Rev. B* **80**, 214415 (2009).
- [38] J. P. Perdew, K. Burke, and M. Ernzerhof, Generalized gradient approximation made simple,

- Phys. Rev. Lett. **77**, 3865 (1996).
- [39] G. P. Zhang and Y. H. Bai, Magic high-order harmonics from a quasi-one-dimensional hexagonal solid, Phys. Rev. B **99**, 094313 (2019).
- [40] Y. R. Shen, *The Principles of Nonlinear Optics*, John Wiley & Sons, Inc., Hoboken, New Jersey (2003).
- [41] C. Kittel, *Introduction to Solid State Physics*, 7th Ed. John Wiley & Sons, Inc., New York (1996).
- [42] G. P. Zhang, G. Lefkidis, M. Murakami, W. Hübner and T. F. George, *Introduction to Ultrafast Phenomena: From Femtosecond Magnetism to High-Harmonic Generation*, CRC Press (2020).
- [43] P. I. Sorantin and K. Schwarz, Chemical bonding in rutile-type compounds, Inorg. Chem **31**, 567 (1992).
- [44] I. I. Mazin, D. J. Singh, and C. Ambrosch-Draxl, Transport, optical, and electronic properties of the half-metal CrO₂, Phys. Rev. B **59**, 411 (1999).
- [45] Q. Zhang, A. V. Nurmikko, G. X. Miao, G. Xiao, and A. Gupta, Ultrafast spin-dynamics in half-metallic CrO₂ thin films, Phys. Rev. B **74**, 064414 (2006).
- [46] S. Mukamel, *Principles of Nonlinear Optical Spectroscopy*, Oxford University Press, New York (1995).
- [47] G. Vampa, C. R. McDonald, G. Orlando, D. D. Klug, P. B. Corkum and T. Brabec, Theoretical analysis of high-harmonic generation in solids, Phys. Rev. Lett. **113**, 073901 (2014).
- [48] O. Neufeld, D. Podolsky, and O. Cohen, Floquet group theory and its application to selection rules in harmonic generation, Nat. Comm. **10**, 405 (2019).
- [49] W. H. Cloud, D. S. Schreiber, and K. R. Babcock, X-ray and magnetic studies of CrO₂ single crystals, J. Appl. Phys. **33**, 1193 (1962).
- [50] G. P. Singh, S. Ram, J. Eckert, and H.-J. Fecht, Synthesis and morphological stability in CrO₂ single crystals of a half-metallic ferromagnetic compound, J. Phys.: Conf. Ser. **144**, 012110 (2009).
- [51] M. Pathak, H. Sims, K. B. Chetry, D. Mazumdar, P. R. LeClair, G. J. Mankey, W. H. Butler, and A. Gupta, Robust room-temperature magnetism of (110) CrO₂ thin films, Phys. Rev. B **80**, 212405 (2009).
- [52] B. J. Thamer, R. M. Douglass and E. Staritzky, The thermal decomposition of aqueous chromic acid and some properties of the resulting solid phases, J. Am. Chem. Soc. **79**, 547 (1957).

TABLE I: Optimized structural parameters of CrO₂. Cr atoms are at ($2a$) positions, (0,0,0) and ($\frac{1}{2}, \frac{1}{2}, \frac{1}{2}$), and O atoms at ($4f$) positions, ($u, u, 0$), ($\bar{u}, \bar{u}, 0$), ($\frac{1}{2} + u, \frac{1}{2} - u, \frac{1}{2}$), and ($\frac{1}{2} - u, \frac{1}{2} + u, \frac{1}{2}$). Our theoretical values are listed under “Theory”, with the experimental ones in parenthesis. Our theoretical u is 0.303, in good agreement with the experimental $u = 0.301 \pm 0.004$ [49]. The experiment lattice constants are $a = 4.4218 \text{ \AA}$ and $c = 2.9182 \text{ \AA}$ [49], $a = 4.423 \text{ \AA}$ and $c = 2.918 \text{ \AA}$ [50], $a = 4.421 \text{ \AA}$ and $c = 2.916 \text{ \AA}$ [51], and $a = 4.421 \text{ \AA}$ and $c = 2.916 \text{ \AA}$ [52]. We adopt the experimental lattice constant from Cloud *et al.* [49].

Atom	x		y		z	
	Theory	Experiment	Theory	Experiment	Theory	Experiment
Cr ₁	0	(0)	0	(0)	0	(0)
Cr ₂	$\frac{1}{2}$	($\frac{1}{2}$)	$\frac{1}{2}$	($\frac{1}{2}$)	$\frac{1}{2}$	($\frac{1}{2}$)
O ₁	0.303	(0.301)	0.303	(0.301)	0	(0)

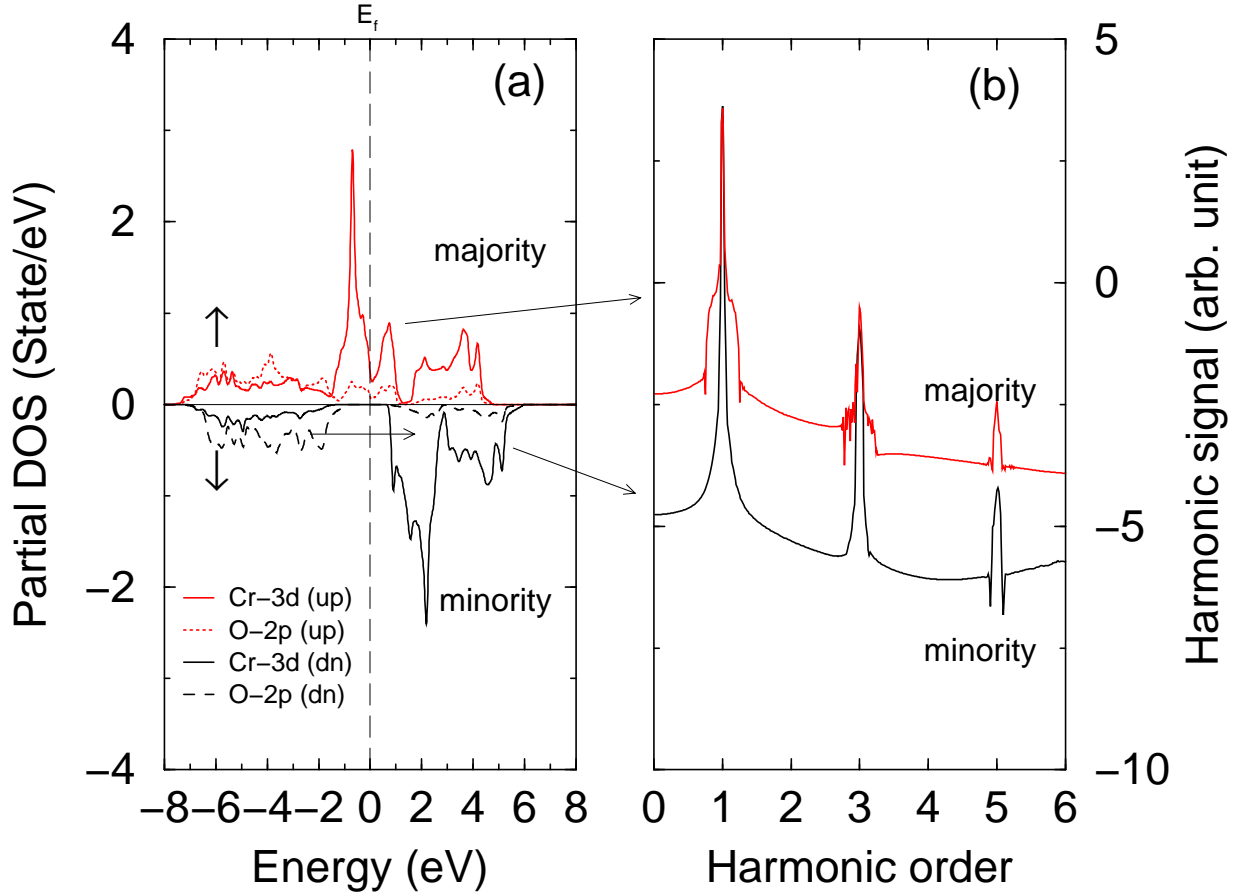


FIG. 1: (a) The partial density of states (PDOS) for Cr-3d and O-2p states for the majority (thick solid and dotted lines on the positive axis) and minority spins (solid and dashed lines on the negative axis). The vertical dashed line denotes the Fermi energy. (b) Logarithmic scale of harmonics from the majority and minority spin channels. Here we use the laser duration of 64 cycles of laser period. The photon energy is 0.4 eV and the laser field amplitude A is 0.03 Vfs/Å. A circularly polarized pulse is used.

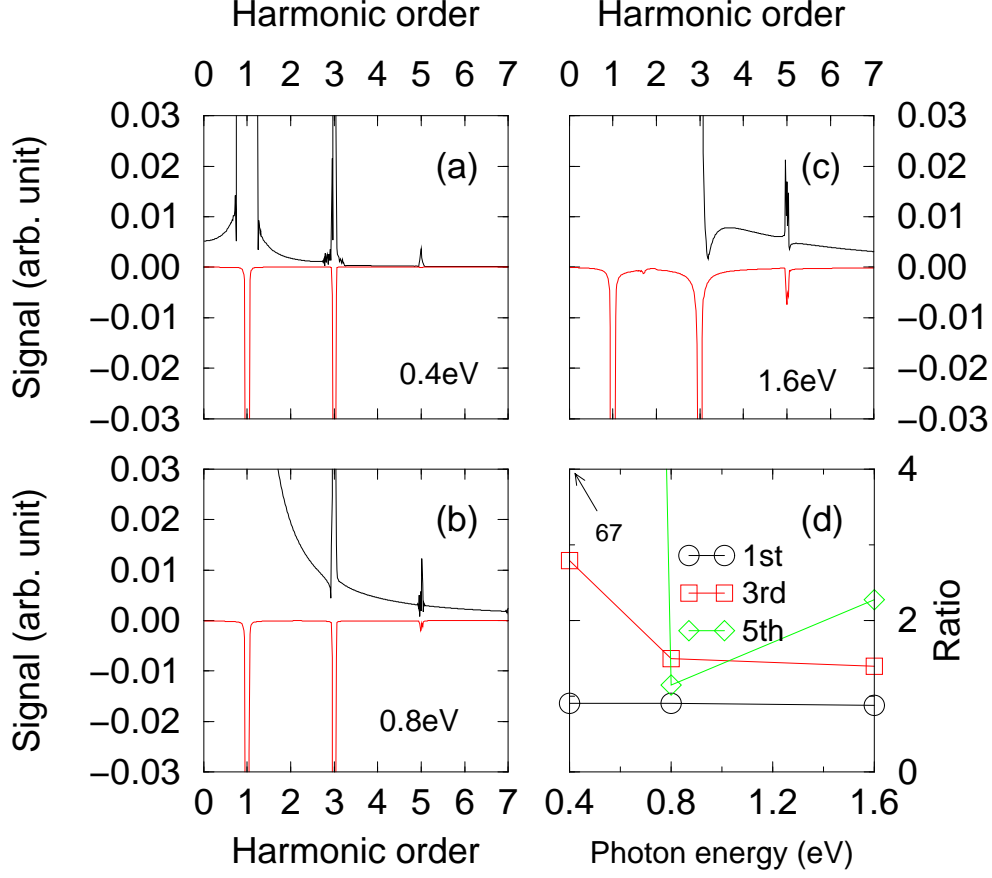


FIG. 2: Dependence of harmonics on photon energies $\hbar\omega$ (a) 0.4 eV, (b) 0.8 eV and (c) 1.6 eV. We choose the vector potential $A_0 = 0.03\text{Vfs}/\text{\AA}$ and the duration of the laser pulse is 64 cycles of laser period. Harmonics from the minority channel are plotted on the negative axis. (a) At 0.4 eV, the majority and minority spin channels produce a similar signal strength at the 1st and 3rd orders, but differ a lot at the 5th order, where the majority dominates over the minority spin channel. This presents an opportunity to generate harmonic mainly from a single spin channel. As we increase photon energy to 0.8 eV (b), the minority 5th harmonic increases its signal strength, so it starts to compete with that from the majority channel. This trend continues as we increase the photon energy to 1.6 eV (c), where the majority and minority channels have a similar strength. (d) Ratio of the majority harmonic signal to the minority harmonic signal as a function of photon energy for the first (circles), third (squares) and fifth (diamonds) harmonics. At 0.4 eV, the ratio for the fifth harmonic reaches 67.

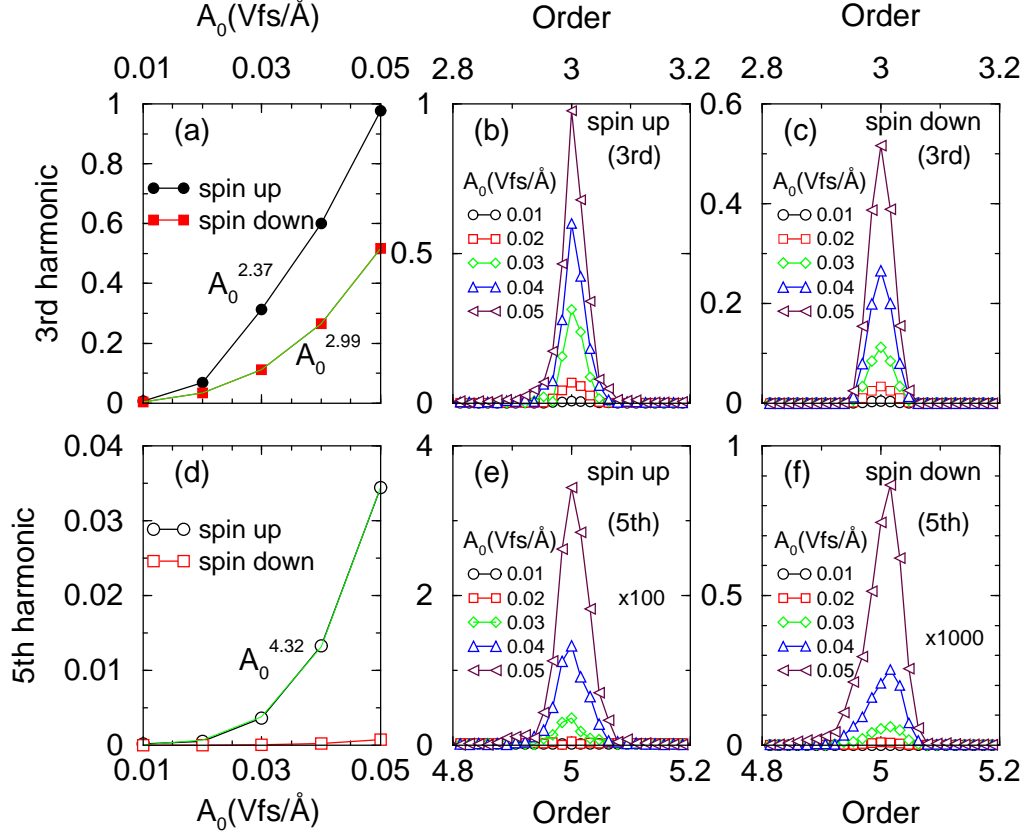


FIG. 3: Dependence of harmonic signals on the laser field amplitude A_0 . The photon energy is 0.4 eV, and pulse duration is 64 cycles of the laser period. Here we use a dense k mesh of $29 \times 29 \times 45$. (a) Third-order harmonics as a function of A_0 for spin up (filled circles) and spin down (filled boxes), which are fitted to a power of $A_0^{2.37}$ and $A_0^{2.99}$. (b) Third harmonic from the spin up channel. The circles, boxes, diamonds, upper triangles and left triangles denote $A_0 = 0.01, 0.02, 0.03, 0.04$ and 0.05 Vfs/Å, respectively. (c) Third harmonic from the spin down channel. All the legends have the same meaning as those in (b). (d) Fifth-order harmonics as a function of A_0 for spin up (filled circles) and spin down (filled boxes). The spin up signal can be fitted to a power of $A_0^{4.32}$. (e) The fifth harmonic from the spin up channel. Here all the signals are multiplied by 100 for an easy view. All the legends have the same meaning as those in (b). (f) Fifth harmonic from the spin down channel. Here all the signals are multiplied by 1000. All the legends have the same meaning as those in (b).

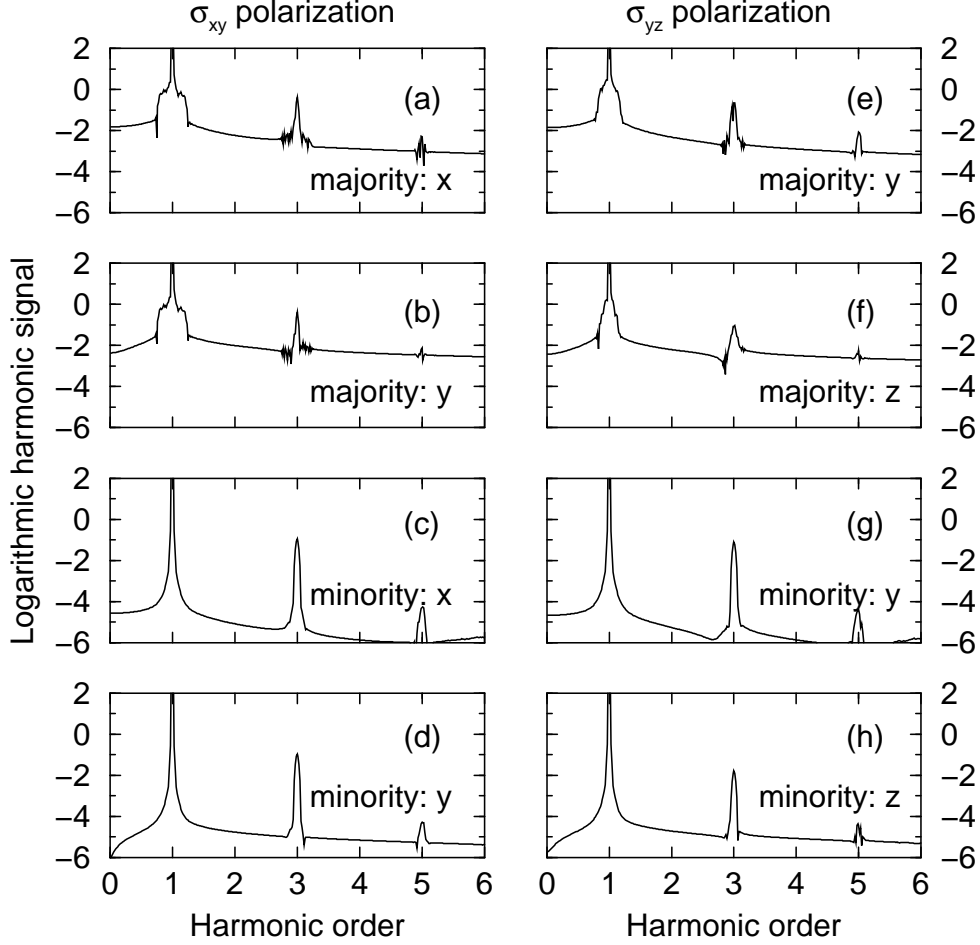


FIG. 4: Influence of relaxation times and laser polarization on harmonics. (a)-(d) use a different set of relaxation times, $T_1 = 400$ and $T_2 = 200$ fs with laser polarization within the xy plane. (a) and (c) show the majority and minority harmonic signals along the x direction respectively, which should be compared with those in Fig. 1(b) with $T_1 = 200$ and $T_2 = 100$ fs. (b) and (d) show the majority and minority harmonic signals along the y direction, respectively. (e)-(h) use the laser polarization in the yz plane with $T_1 = 400$ and $T_2 = 200$ fs. (e) and (g) show the majority and minority harmonic signals along the y direction, respectively. (f) and (h) show the majority and minority harmonic signals along the z direction, respectively. For all the figures, the photon energy is 0.4 eV, the pulse duration is 64 cycles of the laser period and the laser field amplitude A_0 is 0.03 Vfs/Å.